International Journal of Pressure Vessels and Piping 202 (2023) 104875

Contents lists available at ScienceDirect

International Journal of Pressure Vessels and Piping

journal homepage: www.elsevier.com/locate/ijpvp

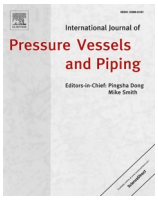

Development and performance of INCONEL® alloy 740H® seam-welded piping

John Shingledecker [a,*], John (Jack) deBarbadillo [b], Ronnie Gollihue [b], Eeva Griscom [a], Dan Purdy [a], Alex Bridges [a]

[a] Electric Power Research Institute (EPRI), Charlotte, NC, USA
[b] Special Metals Corporation, Huntington, WV, USA

ARTICLE INFO

Keywords:
Inconel 740H
Creep
Low cycle fatigue
Seam weld
Microstructural evolution

ABSTRACT

INCONEL® alloy 740H® is an age-hardenable nickel-based alloy approved for pressure vessels and piping within ASME Section I, VIII, and B31.1. Currently, the code applies a weld strength reduction factor (*WSRF*) of 0.7 to the allowable stresses for longitudinal seam welds in the time dependent creep regime. In this work, a full-scale seam weld was successfully produced using typical industrial practices. The component was solution heat-treated and aged after fabrication to improve the performance of the weldment. Tensile, bend, impact, and low-cycle fatigue tests showed the component met all the specification requirements and elevated temperature properties were within base metal expectations with failures predominately in the weld metal. Long-term creep tests, including large samples more representative of the entire weldment, were fabricated and tested to times in excess of 10,000 h at multiple temperatures. Analysis of the creep data supports a *WSRF* of 0.9 for the solution annealed + aged weldments in contrast to the *WSRF* of 0.7 currently applied to welded + aged weldments. Metallurgical analysis shows that the solution annealing causes recrystallization of the weld metal and reduces the chemical compositional and microstructural gradients in the weldments resulting in acceptable short-term performance. In long-term creep, evidence for coarsened zones in the weldments due to discontinuous coarsening reactions were identified as the mechanism leading to accelerated creep damage formation in the weld metal and sample failure.

1. Introduction

INCONEL® Alloy 740H® (UNS N07740, here-in referred to as alloy 740H) is an alloy used in high-temperature pressure boundary applications including advanced thermal steam cycles (i.e., advanced ultra-supercritical), supercritical carbon dioxide power cycles, and concentrating solar power [1–4]. The alloy is one of the highest creep strength materials available to designers for applications up to 800 °C in boilers, heat exchangers, powerplant piping, and valve bodies with code case (CC) approvals in the American Society of Mechanical Engineers (ASME) Boiler & Pressure Vessel Code (B&PV) sections I, VIII, B31.1, and B16 [5–8]. The ASME B&PV CC's for alloy 740H state that ' … *when a longitudinal weld seam is required in the construction of a component, a weld strength reduction factor (WSRF) of 0.7* shall *apply … at temperatures above 600°C …* [5]'. Seam weld piping is of strong interest in advanced power cycles due to flexibility to create custom pipe size and large diameter thinner wall piping which is costly or impossible to fabricate using traditional extrusion process [9]. However, a *WSRF* of 0.7 effectively requires increasing wall thickness by 30% for applicable components negating many of the likely benefits. Thus, there is a strong driver to explore options for improving the creep performance of alloy 740H weldments.

Long-term creep testing of alloy 740H weldments using matching 740H filler metal has previously been conducted on a variety of product forms including tubular butt welds and plates using both 740H filler metal with compositions matching the base metal and alternative filler metals [10]. Multiple methods of creep data analysis were used to evaluate the test results which found a *WSRF* of 0.7 (30% reduction in stress to produce rupture at the base metal equivalent time and temperature) was appropriate and largely independent of test duration or applied temperature for aged weldments made with matching filler metal [11,12]. Alternative filler metals were found to improve performance and more recent extensive research with long-term creep tests has shown using a nominally lower creep strength filler metal, alloy 263,

* Corresponding author.
E-mail address: jshingledecker@epri.com (J. Shingledecker).

https://doi.org/10.1016/j.ijpvp.2022.104875
Received 24 October 2022; Received in revised form 15 December 2022; Accepted 22 December 2022
Available online 23 December 2022

resulted in an improvement with only a 15% reduction at 650 and 750 °C, but a larger reduction >25% at 850 °C (i.e., loss of creep resistance) due to rapid gamma prime (γ') coarsening and the formation of eta phase [13]. Preliminary conclusions from a less extensive test campaign on tube butt-weldments of alloy 740H showed applying a solution annealing heat-treatment after welding with matching filler metal could potentially restore the strength of the weldment to near base metal (BM) properties [11].

Bechetti and co-workers have extensively examined the microstructures and response to heat-treatment and creep exposure for alloy 740H weldments and found that for welded + aged materials, compositional gradients (segregation) within the weld metal (WM) provides a driving force for the formation of coarsened zones (CZ) at grain boundaries leading to accelerated creep deformation and failure within the WM [14–17]. These CZ are often described as precipitate free zones (PFZs), but careful observation shows that with applied stress and temperature, the compositional gradients result in moving boundaries which 'leave behind' coarsened or elongated γ′ precipitates and carbides and associated creep weak γ′ denuded regions where creep deformation is concentrated and creep damage (cavitation) initiates. In contrast, creep studies, up to a few thousand hours, of both weldments and simulated heat affected zones (HAZs) in alloy 740H do not show the formation of denuded regions in the HAZ regions of 740H [18].

2. Materials, manufacturing & methods

2.1. Materials & manufacturing

The seam-welded alloy 740H pipe was fabricated by Swepco Tube, Llc. (Clifton, NJ USA) from a 1118 mm wide x 6100 mm long x 19.1 mm thick plate produced by Special Metals Corporation (Huntington, WV USA), heat HT6309JK, weighing 1174 kg. The gas tungsten arc welding (GTAW) process was used with matching 1.1 and 1.6 mm diameter alloy 740H filler wire, heat HT5502JY. Utilizing a double-v-groove weld joint design, a total of ten passes were required. Interpass temperature was maintained at or below 177 °C. To minimize oxide buildup during welding and minimize occurrence of Lack-Of-Fusion (LOF) type discontinuities, individual weld passes were abrasively skim ground to remove the thin oxide layer that forms during welding. Following welding, the pipe was solution annealed at 1107 °C for 47 min and water quenched. It was then was aged at 800 °C for 240 min and air cooled. Table 1 provides the chemical composition and Fig. 1 shows images of the pipe during and after fabrication.

2.2. Experimental procedures

Non-destructive evaluation (NDE) of the pipe was conducted in accordance with ASTM B775 [19] including radiography (RT) per ASME Section VIII paragraph UW51 [20], dye penetrate, and ultrasonic (UT) to ASTM E213-02/ISG-UT 500 Rev 10 [21]. Destructive acceptance testing included room temperature tensile testing and bend testing per ASME Section IX [22]. Additionally, room and elevated temperature tests were conducted in accordance with ASTM E8 [23] in multiple orientations longitudinal and transverse to the weld seam and impact tests were conducted in the BM, WM, and HAZ. Low-cycle fatigue (LCF) testing was conducted on 6.35 mm gauge diameter cross-weld samples with the weld centered in gauge. Testing was conducted in strain control with an R-ratio of −1 to ASTM E606-19 at a frequency of 0.3 Hz and test termination when the maximum stabilized stress dropped by ~30%, fracture occurred, or 200,000 cycles were reached (run-out) [24]. Creep-rupture tests were conducted in accordance with ASME E139 [25] in lever-arm creep frames with the exception that alternative larger cross-section specimen designs encompassing both the BM and WM as shown in Fig. 2, were utilized. For the largest sample design to accommodate the arc of the pipe, solid alloy 740H tabs were welded onto each end of the removed arc prior to machining. These new tab welds were placed in the threaded region of the sample away from the gauge section so as not to affect any test results. The use of large sample cross-weld samples provides a much larger volume of WM so that each sample contains multiple weld beads, near root, and cap regions. Table 2 provides a summary of the sample sizes used for creep testing. Such samples have been shown to be more representative of the complex stress redistributions and damage which occur during creep in components for some alloys and allows for post-test macro-evaluations of a relevant weldment cross-sections [26–28]. Elevated temperature testing was conducted for temperatures between 600 and 850 °C to provide both service relevant performance data and accelerated testing for long-term creep prediction up to the maximum use temperature of the alloy which is currently 800 °C. Prior research with long-term creep testing up to 875 °C on alloy 740H wrought products is the basis for the current stress allowables in ASME.

2.3. Metallographic examination

Pre- and post-test metallographic preparation consisted of polishing samples using standard procedures to a final polish of 0.4 μm with colloidal silica. Light optical microscopy was conducted on using a high-resolution digital microscope (Keyence VHX-7000). Select samples for optical metallography were etched using a 2% bromine - 98% methanol solution or electrolytically using 10% oxalic acid. Micro-hardness mapping was conducted on select samples using a Vicker's indenter at a 500 g load with a spacing of 250 μm or 350 μm depending on map size. Select samples were etched electrolytically using 2% nital in preparation for scanning electron microscopy (SEM) using an FEI Teneo FEG-SEM in backscatter electron imaging (BSE) mode. Energy dispersive spectroscopy (EDS) was conducted using an Oxford Ultimax Si Drift Detector with the accompanying Oxford Aztec analysis software. Additionally, electron backscatter diffraction (EBSD) was completed using a Hikari Pro high-speed EBSD detector and accompanying EDAX Teams software.

3. Calculations

To characterize the mechanical response of a weldment to creep, a *WSRF* is calculated by comparing the rupture strength or stress to produce rupture (σ_r) at a given temperature (T) and time (t_r) for a weldment to the unwelded BM as follows:

$$WSRF = \frac{\sigma_r^{weldment}(T, t_r)}{\sigma_r^{base\ metal}(T, t_r)} \quad (1)$$

There is not a universal agreement on the best method of data analysis to determine a *WSRF*, so two different approaches were taken for this analysis. This first was to calculate an individual *WSRF* for each completed weldment test by comparing the applied stress to the calculated average stress for rupture of the BM at the measured rupture time

Table 1
Chemical composition (wt%) of alloy 740H materials in this study compared to UNS specification minimums (Min) and maximums (Max).

Heat ID	C	Mn	Fe	S	Si	Cu	Ni	Cr	Al	Ti	Co	Mo	Nb	P	B	N	W
UNS N07740 -Min	0.005							23.5	0.2	0.5	15.0		0.5		0.0006		
UNS N07740 -Max	0.08	1.0	3.0	0.03	1.0	0.50	Bal	25.5	2.0	2.5	22.0	2.0	2.5	0.03	0.006		
HT6309JK (plate)	0.033	0.29	0.17	0.0005	0.15	0.02	49.73	24.59	1.4	1.48	20.03	0.49	1.51	0.007	0.002	0.0043	0.045
HT5502JY (wire)	0.034	0.24	0.17	0.0010	0.15	0.03	49.48	24.56	1.45	1.46	20.35	0.48	1.48	0.008	0.002	0.0053	0.047

Fig. 1. Pipe during fabrication (left) and finished pipe (right).

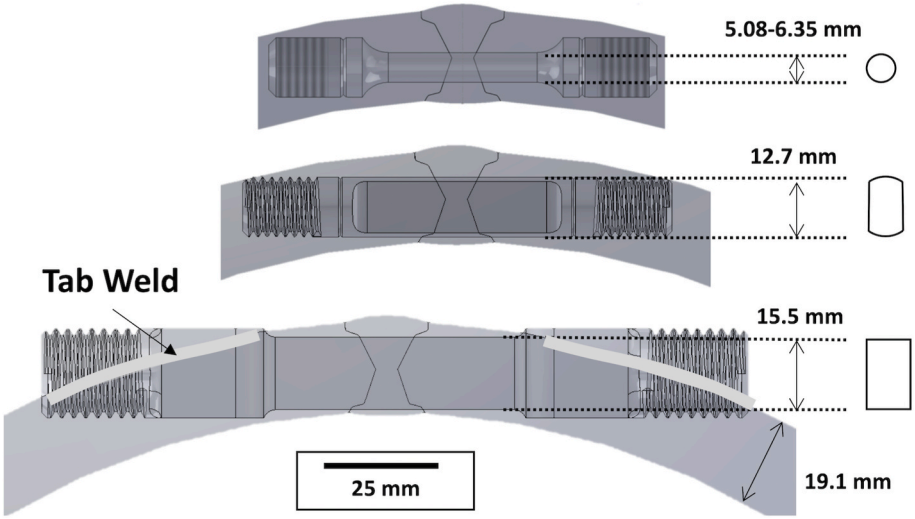

Fig. 2. Cross-weld creep sample designs.

Table 2
Cross-weld sample gauge sizes.

Sample designation	Maximum sample gauge dimension (mm)	Percentage of actual weld thickness tested	Cross-sectional area (mm^2)	Relative tested area of weld compared to standard
Standard ASTM round bar	5.08 - 6.35	27–33%	32.3	1
Modified 12.7 mm diameter	12.7	66%	77.4	2.4
Welded end-tab rectangular cross-section	15.5	80%	129	4

of the weldment. The second was to develop a fit to the weldment results using a time-temperature parameter approach. This fit was then used to calculate the stress to produce rupture in 100,000 h and compared to BM average behavior at 100,000 h. For fitting both the base metal and weldment rupture data, a lot-centered Larson Miller Parameter (*LMP*) approach, which is one of the preferred methods applied by ASME for determination of allowable stresses, was utilized as described in Refs. [29,30]. The regression analysis was conducted to minimize the error in stress to the following where C is the *LMP* constant, a_X are the regression coefficients, and T is temperature in Kelvin.

$$\log(t_r) = -C + \frac{a_0}{T} + \frac{a_1}{T}\log(\sigma_r) + \frac{a_2}{T}\log(\sigma_r)^2 + \frac{a_3}{T}\log(\sigma_r)^3 \quad (2)$$

The LMP is defined as:

$$LMP = T \times (\log(t_r) + C) \quad (3)$$

The *LMP* approach has been applied to wrought alloy 740H and found to be a good predictor of long-term rupture life when compared to other methods of analysis [31,32]. The base metal database used for this analysis involved expanding an earlier data set from Ref. [31] with additional base metal data from Refs. [32–35], and the weldment database utilized the data from this study combined with previously reported data on solution annealed + aged tube butt welds [10,11].

4. Results

4.1. Weld fabrication and testing

As shown in Fig. 1, the seam weld was successfully welded and heat-treated. Post-fabrication NDE RT and UT did not indicate any cracking, slag, or LOF defects. RT did reveal WM indications as isolated porosity below the rejection threshold for the applicable standards. Fig. 3a and b shows examples of both isolated surface and weld metal porosity which were all measured less than 100 μm which is well below the 20% of wall thickness or 3 mm acceptance criteria. Room temperature cross-weld

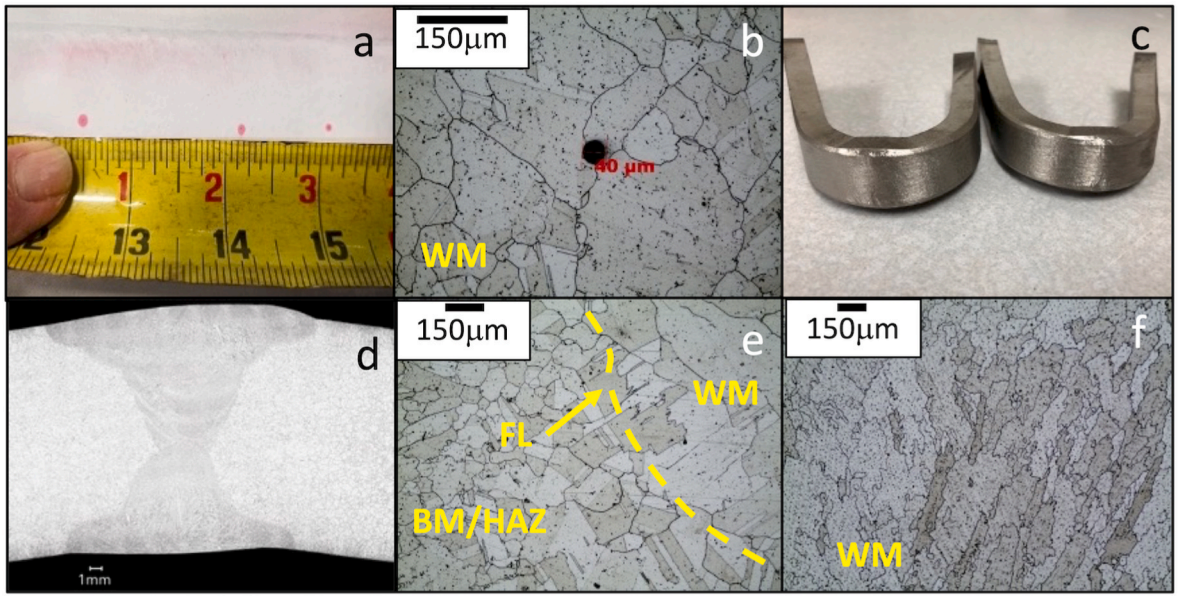

Fig. 3. Isolated non-rejectable surface (a) and WM (b) porosity (40 µm diameter pore indicated); example of successful bend tests (c); macro showing overall weld geometry and structure (d), and representative micrographs of the FL region (e) and WM (f) showing recrystallization and no evidence of microfissures, LOF, cracking or other weld defects.

tensile tests met the minimum BM criteria with ductile fracture and all four side-bend tests, examples shown in Fig. 3c, passed the qualification. Supplementary 2 T side and face bends were conducted and all passed confirming the porosity was not impacting room temperature ductility. Additional room and high-temperature tensile tests were conducted and the results, Fig. 4, show all the yield strength (YS) results exceeded the ASME tensile trend curves and, with the exception of some of the data at 600–650 °C, all the tests met or exceeded the ASME ultimate tensile strength (TS) value. Room temperature tensile elongation values all exceeded the specified minimum of 20% with an average cross-weld elongation of 33.8%. Table 3 provides the impact test results where relatively high impact values were obtained for all locations and orientations in the pipe. Fig. 3d provides cross-sectional image of the weld showing no macro defects and 3e and 3f show representative recrystallized microstructures in the WM and fusion line (FL) regions without any welding related defects such as cracking, large inclusions, or microfissures.

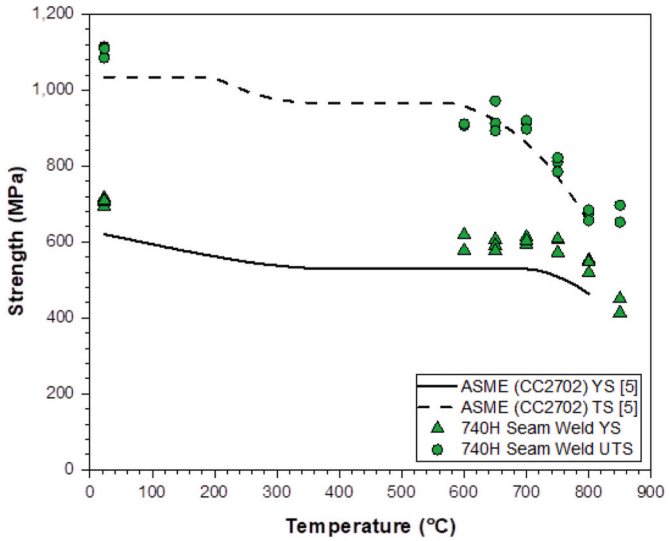

Fig. 4. Tensile test results for the alloy 740H seam weld.

Table 3
Charpy-V notch impact test results.

Weldment Region	Orientation/Location	Impact Energy (J)
Base Metal	Longitudinal	86.4, 112.4, 126.8
Base Metal	Transverse	104.7, 104.7, 107.7
Weldment	HAZ	101.8, 101.3, 104.8
Weldment	WM	101.8, 81.9, 83.7

4.2. *High-temperature testing*

Duplicate LCF tests transverse to the alloy 740H pipe seam weld were conducted at room temperature, 750 °C, and 850 °C for three total strain

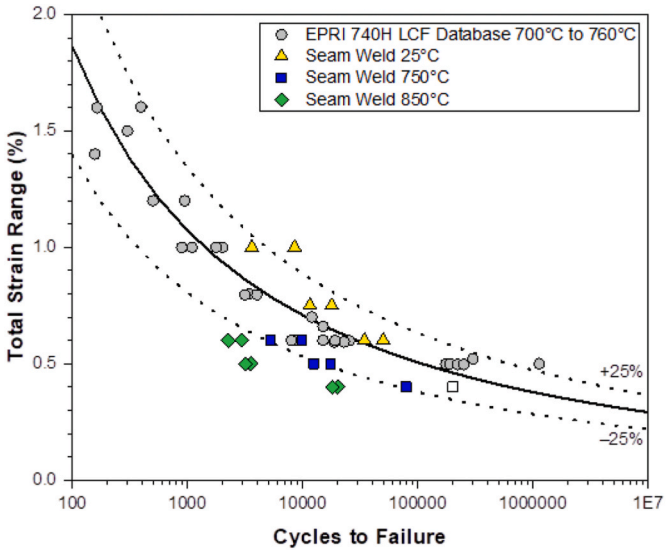

Fig. 5. LCF test results for alloy 740H cross-weld samples tested at room temperature (triangles), 750 °C (squares), and 850 °C (diamonds) compared to the EPRI wrought 740H LCF database (circles) which is combination of data from Refs. [33,34,36,37], open symbols represent tests which were stopped prior to failure (run-out condition).

ranges to produce cycles-to-failure between 1000 and 100,000 cycles. The results from this pipe are shown in Fig. 5 and are compared to the wrought alloy 740H strain range vs. cycles to failure data and fit curve from the EPRI database spanning data collected at 700–760 °C from Refs. [33,34,36,37]. At 750 °C, the seam weld data showed behavior ~20% below the wrought data, placing it at the lower end of the wrought material scatter band; however, the welded samples demonstrated some degree of strain localization in or near the weld which might increase the local strain conditions relative to the global test conditions. The figure shows the global test conditions. Post-test fractography found most cracking initiating at the surface of the sample in the weld metal. Testing at room temperature improved cyclic performance while testing at 850 °C resulted in shorter cycle life at the equivalent strain ranges. Thus, the results show that the WM is inferior to the BM in LCF but still within overall expections.

Creep-rupture tests were conducted from 700 to 850 °C for times up to ~14,000 h. These data are shown in Table 4 which provides in total approximately 72,000 h of test data. Creep-strain was measured for all tests but is not reported since it represents a composite strain rate of BM, HAZ, and WM. The data are segmented by sample (Fig. 2) design and no clear trend was observed based on sample geometry, although only a few standard samples were evaluated. Ductility appears to increase slightly as testing temperature increases and some of the longer-term tests for a given temperature show a slight decrease in ductility, but overall, the elongation and reduction of area are comparable across conditions. Fig. 6 plots the time-to-rupture data using the LMP (Equation (3)) using a previously reported optimized LMP constant of C = 19.392 [11]. These data are compared to the expected wrought alloy 740H average behavior as well as the average −30%, data on welded + aged alloy 740H, and past data on solution annealed + aged tube butt weldments.

4.3. Microstructural findings

The seam welded pipe cross-weld rupture lives are comparable to the past research on the SA + aged weldments which is slightly below the average wrought life. The failure location for all the seam-weld creep tests was in the weld metal as shown in failure atlas's for unetched metallurgical cross-sections of tested creep samples in Figs. 7 and 8. Inspection of the figures show that for higher stresses and temperatures (generally at 700 and 750 °C and stresses above 200 MPa), damage occurs mainly in the weld metal as isolated creep cavities with minimal growth of microcracks and failure due to a single macro crack. Conversely at lower stresses below ~200 MPa and tests at or above 750 °C, damage is more widespread including both FL and WM cavitation with extensive microcracking leading eventually to macro cracking and failure. Fig. 9 shows the micro-hardness distribution for the weldment and selected creep tested samples and Fig. 10 provides the statistical distribution of the measured BM hardness. BM hardness was plotted instead of the entire weldment because all failed sample showed significant hardness increases near the failure location (which was in the weld or near the FL) due to plastic straining during the final failure process. Overall, these plots show hardening of the material at 700 °C, minimal hardness change at 750 °C, and decreased hardness at 800 °C.

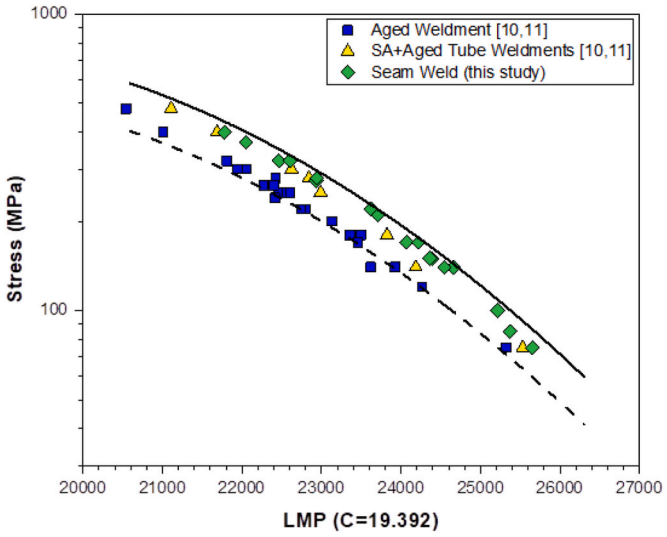

Fig. 6. LMP (C = 19.392) plot for alloy 740H seam welds compared to average base metal (solid line) and 30% reduction on stress (dashed line). Data for previous research on weldments made with matching filler metal for both welded + aged (Aged Weldment) and welded + solution annealed + aged (SA + Aged Tube Weldments) are included for comparison [10,11].

Fig. 11 provides a comparison of the characteristic microstructures observed after long—term creep testing in the region of grain boundaries for the BM, FL, and WM regions. At 750 °C, the grain interiors of all regions show very fine spherical γ′precipitates which after similar time exposure at 800 °C coarsen and show some agglomeration. Grain boundaries in the BM are covered with relatively fine precipitates. Conversely, the FL and WM show significant coarsening of grain boundary precipitates has occurred and some regions appear to have PFZ with no γ′or carbides. In some instances, creep cavities (see bottom middle image in Fig. 11) are identified in these regions. Fig. 12 shows the appearance of creep cavities within the denuded regions of grain boundaries in weld metal after creep testing. Extensive compositional

Table 4
Creep-rupture test results.

Sample Design	Stress (MPa)	Temperature (Celsius)	Time to Rupture (hours)	Elongation (%)	Reduction of Area (%)
15.5 mm Welded end-tab rectangular cross-section	400	700	967.2	3.3	8.3
	320	700	4906.8	3.8	12.1
	275	700	14873.1	2.1	5.3
	320	750	497.5	6.2	14.4
	280	750	1071.8	6.3	13.9
	220	750	4981.3	2.1	7.9
	170	750	13530.7	3.3	5.7
	150	850	211.0	–	24.6
	140	800	3858.5	2.5	12.5
	170	800	1492.2	7.1	20.9
	100	800	12690.0	16.1	4.8
Modified 12.7 mm diameter	210	800	502.6	7.4	14.6
	150	850	199.6	20.5	15.4
	140	850	291.1	9.0	11.5
	75	850	2793.0	3.5	2.8
	85	825	5128.0	7.2	9.8
Standard ASTM Round Bar 0.2″ Diameter	370	750	144.1	6.7	15.8
	313.7	750	517.5	6.8	14.2

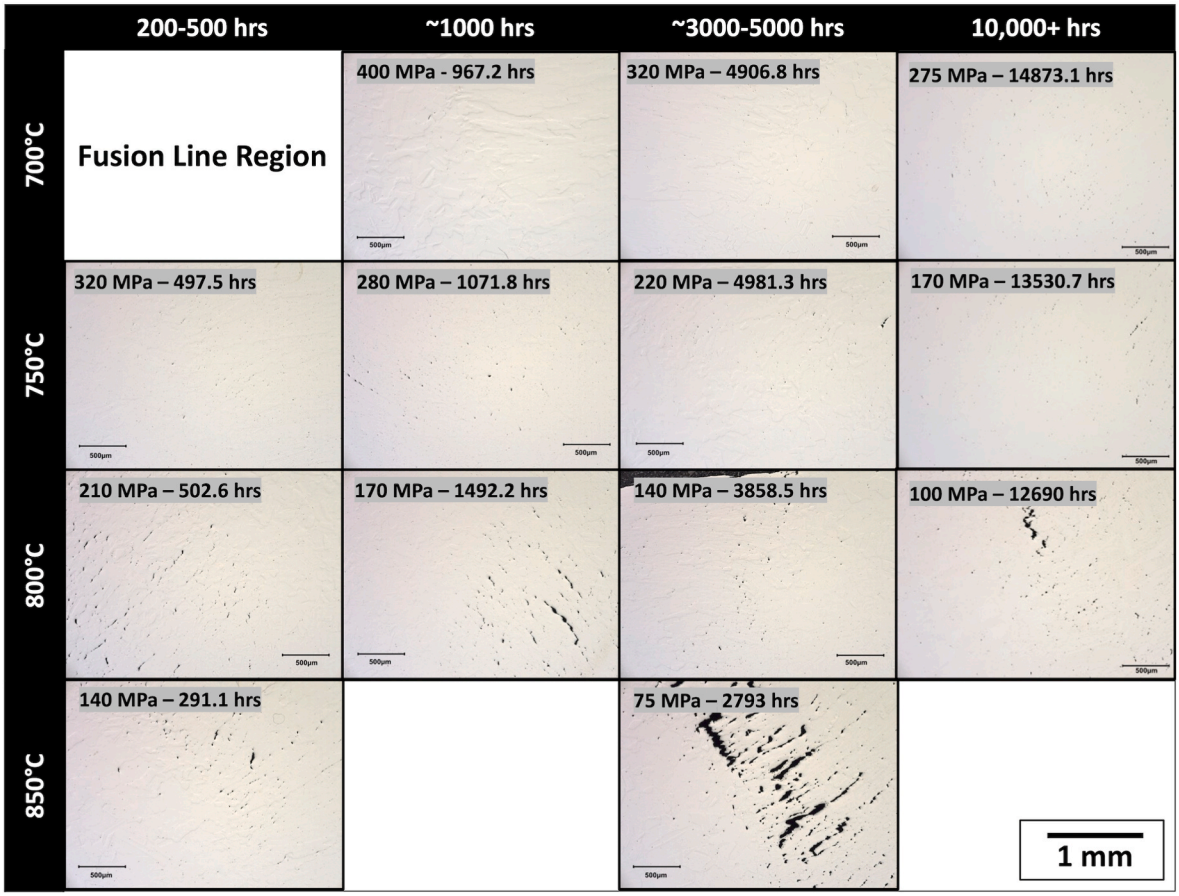

Fig. 7. Unetched micrographs of the FL regions including HAZ and WM after creep testing showing creep damage. Applied stress is in the horizontal axis.

analysis was not conducted as the general microstructural constituents of alloy 740H are well characterized, but to clarify the grain boundary observations of potential γ′ denuded regions (PFZs and/or CZ), EDS line-scan analysis was conducted. The subsurface volume of interaction in EDS is advantageous for such analysis because grain boundaries are viewed in 2-D but in reality, are complex 3-D shapes. Thus, etching or sample preparation effects which may accentuate the appearance of denuded regions or mask precipitates can be minimized. Fig. 13 shows line scans for three specific regions after creep testing. In the BM, small concurrent undulations of Al, Ti, Nb, and Ni confirm the presence of fine γ′ throughout the grain interior and through the grain boundary. A Cr-rich carbide is observed on the grain boundary as a Cr peak and Ni valley. In the FL region significant concurrent intensity and width increases for the Al, Ti, Nb, and Ni peaks indicate a coarsened γ′ precipitate near the grain boundary as well as a corresponding Cr-rich carbide. Next to this region, the EDS confirms a γ′denuded region (indicated on the images with a horizontal double tail arrow) which is approximately 1 μm in width and characterized by near zero measurements for Al, Ti, and Nb with flat (no peak) profiles for Ni, Cr, and Co. A similar observation is made in the weld metal with the exception that no Cr-rich peak (carbide) was observed.

The regression analysis was conducted on the expanded BM database and the combined seam-weld data from Table 4 and historical data on solution annealed + aged alloy 740H weldments. Overall, the fits were good with R^2 values (goodness of fit) of 0.94 and 0.98 for the BM and weldment respectively. The resultant polynomial equation coefficients are provided in Table 5. Compared to previous analysis which obtained a LMP constant of C = 19.392, the new analysis obtained a C = 19.929887 for the expanded database.

5. Discussion

5.1. Fabrication

The weldability of γ' strengthened alloys can be a challenge due to a range of potential damage mechanisms during the welding and post-welding heat-treatment of weldments [38]. This work clearly shows that with proper control of the fabrication practice, successful fabrication of alloy 740H seam welded pipe is achievable using standard industrial practices. Furthermore, the extensive testing beyond the minimum requirements of the codes and standards in this work show the solution annealed and aged alloy 740H weldments have good room and elevated temperature tensile strength, ductility, and impact resistance. The use of three NDE techniques (two volumetric and one surface), the examination of multiple metallurgical mounts of the fabricated component, and the post-exposure analysis including fractography and cross-sectional metallography of over 60 mechanical test specimens did not identify any inclusions, cracks, LOF, or microfissures in the weldment. The limited porosity in the WM which was observed did not appear to have any impact on time independent mechanical properties likely because the porosity was small and isolated.

5.2. High-temperature performance

The elevated temperature LCF and creep results show that the alloy 740H seam welds fail in the WM and WM + FL regions at cycles and times below the average alloy 740H wrought behavior. The LCF results were at the bottom of the wrought 740H scatter band and the creep-rupture life was, based on literature data, in between weldments which were only given an aging heat-treatment and average wrought

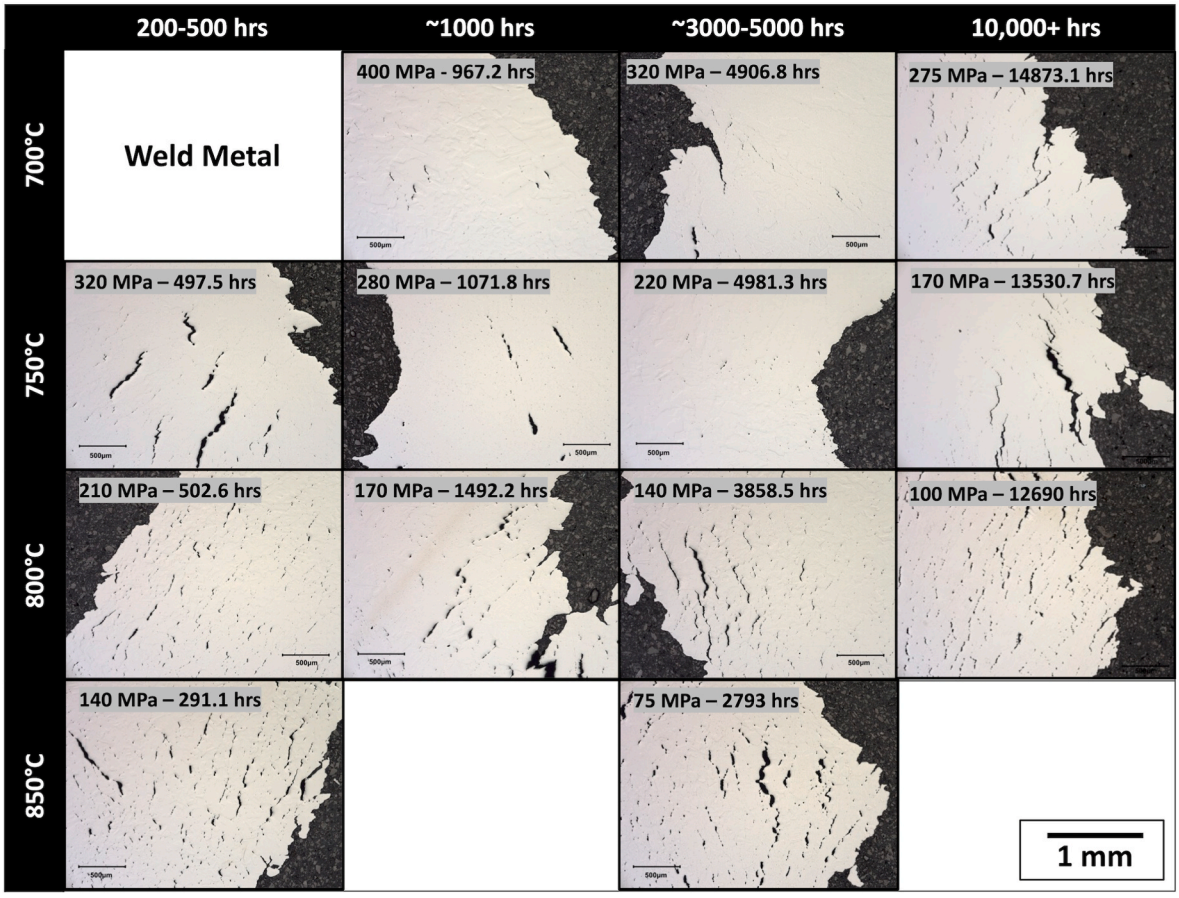

Fig. 8. Unetched micrographs of the WM after creep testing showing creep damage. Applied stress is in the horizontal axis.

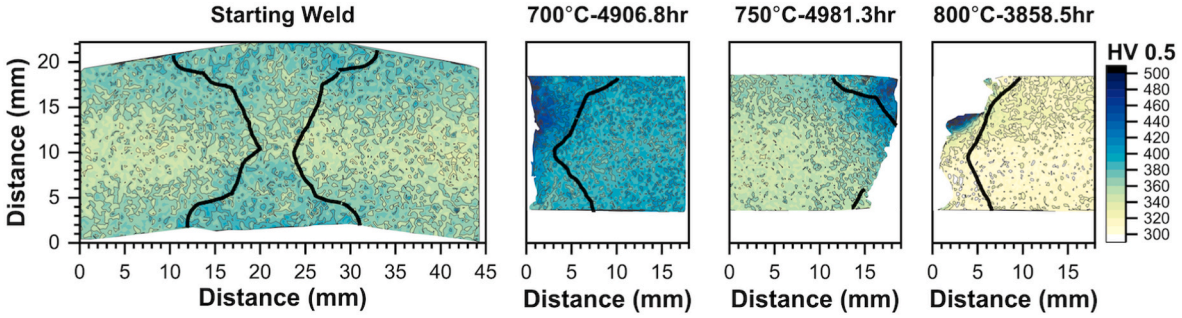

Fig. 9. Weldment hardness distribution for the starting weld and selected samples after creep exposure. Approximate location of the FL is indicated by the solid line for each sample.

life. To explore the *WSRF* (equation (1)) in more detail, Fig. 14 plots the measured *WSRF* for each completed seam weld cross-weld test as a function of rupture life and testing temperature. All of the data show a *WSRF* of 0.90 or greater with most data above 0.95. A single short-term BM creep test was conducted on the pipe at 750 °C which found the starting BM had an equivalent *WSRF* of 1.03 (3% above average wrought behavior) which was greater than any of the cross-weld tests. This may explain why minimal/no creep damage was observed in the BM even when the *WSRF* was nearly unity for some cross-weld test. Further inspection of the data show no trend with testing temperature but a weak negative trend as a function of testing time with longer-term tests trending below a *WSRF* of 0.95 as indicated by the log-linear trend line in Fig. 14a.

As an alternative method for calculation of a *WSRF*, the 100,000 h average rupture life was calculated for the BM database and the cross-weld database (combination of this research and prior research on solution annealed + aged weldments) as shown in Table 6. Using these 100,000 h extrapolations, the resultant *WSRF* was found to be 0.9 for temperatures between 700 and 800 °C with a value of unity for 825 °C. These values are generally more conservative than the individual calculation in Fig. 14. This may be due to the inclusion of additional data in the database or the time-temperature parameter fitting approach utilized. One challenge with using the *LMP* approach with a polynomial expression is the extrapolation of data below the lowest stress in the database. While the goodness of fit values were exceptionally high for this analysis, this only provides a measure of confidence in the stress range of the test data. As indicated in Table 6, the 800 and 825 °C values rely on extrapolation beyond the weldment database. Considering the

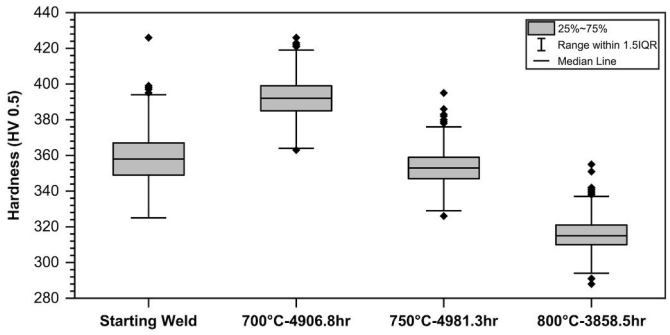

Fig. 10. Post-test base metal hardness distributions (see Fig. 9) with outliers (diamonds). The shaded boxes are defined by the upper and lower quartiles (25%–75%) which are the values halfway between the mean and largest or smallest value respectively, and the outliers are those values falling outside 1.5 times the inner quartile distance (Range within 1.5IQR).

global database analysis (Table 6) and the individual performance of the tests (Fig. 14), a *WSRF* of 0.9 applied to all temperatures in the creep regime appear appropriate and conservative for pressure part design.

5.3. Microstructure

Microstructural evolution during creep testing shows an increase in hardness at 700 °C likely due to additional precipitation of fine γ′whereas the hardness shows little change at 750 °C and significant softening at 800 °C due to γ′coarsening. Inspection of the γ′ in Fig. 11 shows similar fine γ′at 750 °C, but at 800 °C it appears that the strain accumulation from creep in the WM has caused elongation of the γ′precipitates in the grain suggesting a difference in microstructural stability between the regions. More importantly, there are clear differences in the evolution of the grain boundaries after creep testing in the WM and FL regions with the formation of γ′denuded regions leading to extensive creep cavitation and ultimately fracture. The proposed mechanism for denuded regions in alloy 740H after welding + aging is discontinuous γ′coarsening reactions leading to CZs. The driving force for these CZs in the weld metal in comparison to the base metal is likely the inhomogeneous weld metal microstructures including large compositional gradients. During creep, grain boundary sliding and migration occur due to the microstructural gradients leading to the CZs and corresponding γ′ denuded sites for creep damage initiation in the WM while no creep damage is observed in the BM [15,16].

In this study, the seam weld was subject to a solution annealing heat-treatment at 1107 °C for 47 min with the goal of reducing microstructural gradients within the weld metal and thus improving creep performance. However, the EDS data (Fig. 13) confirm the general SEM observations that denuded regions at the grain boundary are associated with large coarsened γ′precipitates, suggesting the solution annealing has not completely eliminated the discontinuous precipitation mechanism and formation of CZs. To confirm the presence of a migrating grain boundary, which is necessary for the proposed mechanism, EBSD was performed to identify the location of the grain boundary relative to the coarsened precipitates and denuded regions. Fig. 15 is an overlay of the EBSD map on a BSE SEM image clearly showing the migration of a grain boundary from ‘grain 1’ into ‘grain 2’ in the region associated with the CZ. Thus, there is clear evidence that solution annealing has not eliminated the damage mechanism for alloy 740H.

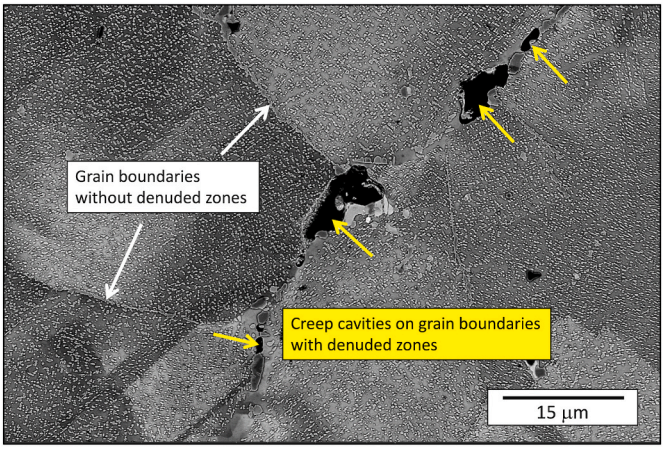

Fig. 12. Creep cavitation in the weld metal after testing at 800 °C for 3858.5hrs. Applied stress is in the horizontal plane.

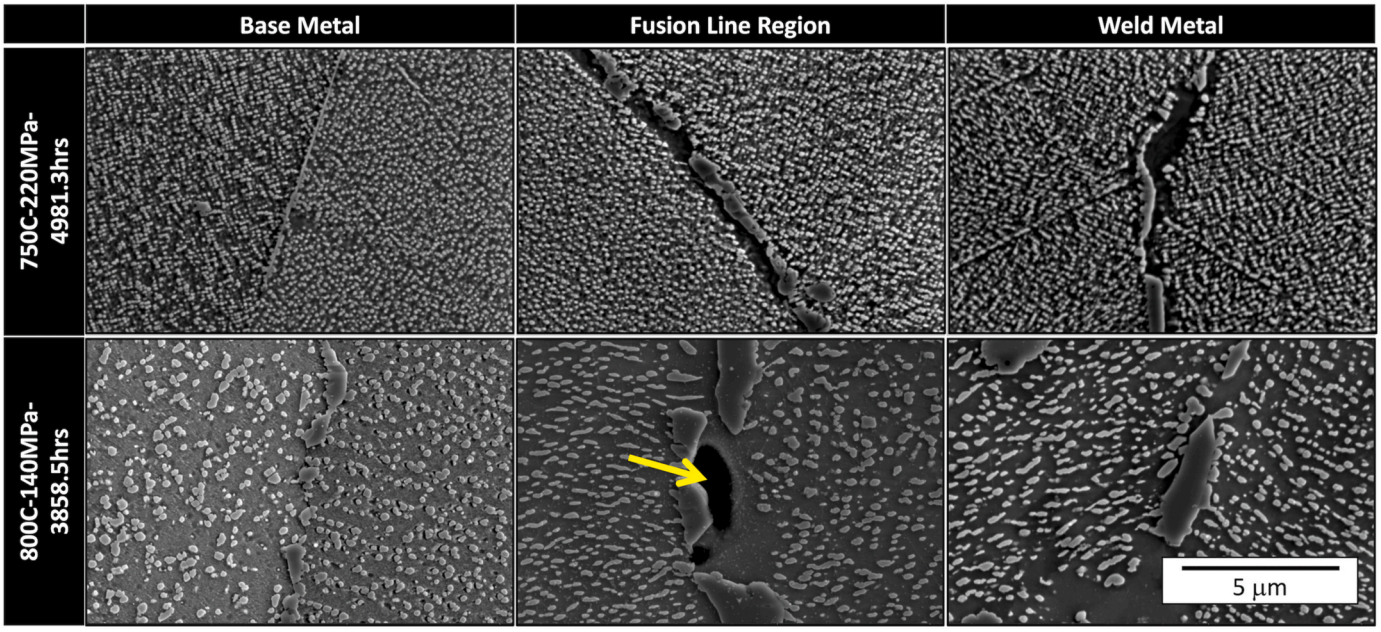

Fig. 11. BSE Images of grain boundaries in the BM, FL, and WM regions after creep testing. Applied stress is in the horizontal plane and the arrow indicates a creep void forming on a grain boundary normal to the applied stress.

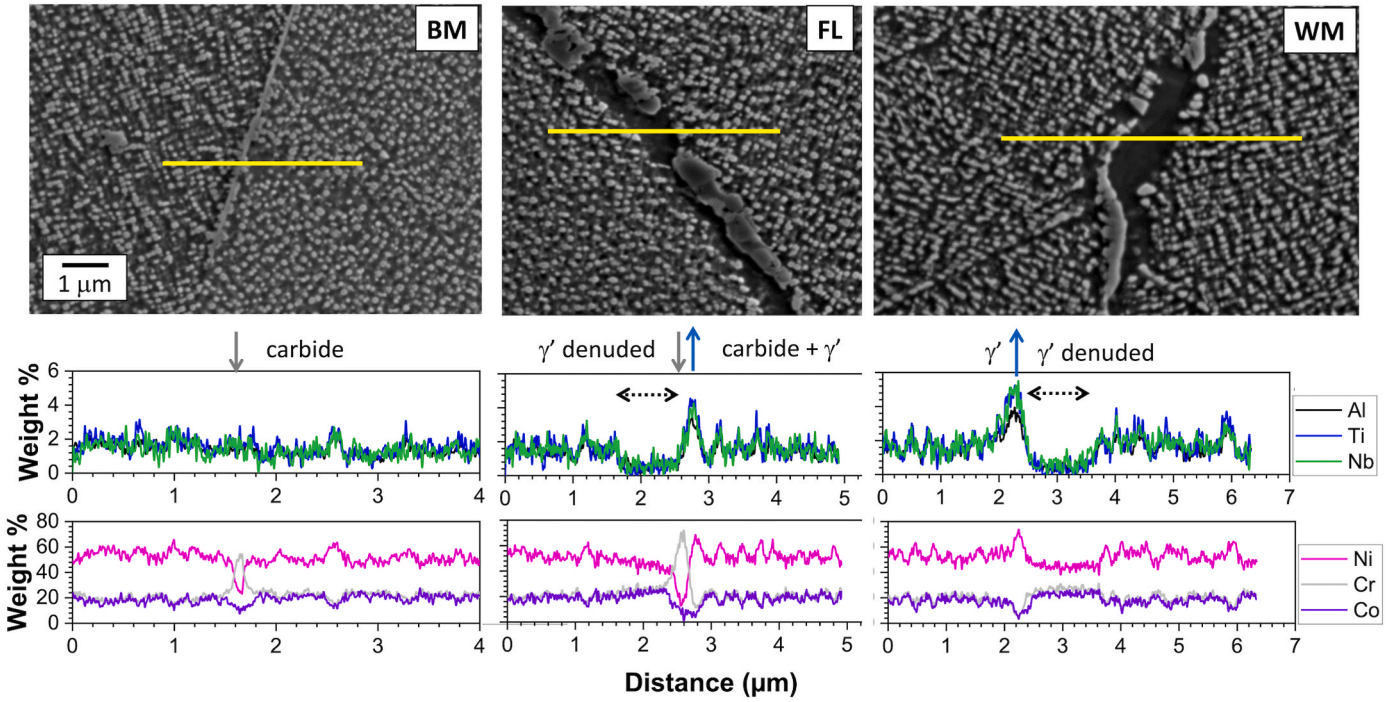

Fig. 13. BSE images with EDS line scans identifying grain boundary carbide formation and coarsened γ′associated with γ′denuded zones in FL and WM regions in contrast to the BM after creep testing at 750 °C for 4981.3 h. Down arrows indicate location of carbides, up arrows γ′, and double ended arrow γ′denuded regions.

Table 5
Results of LMP regression analysis (Equation (2)).

	Base Metal	Weldment
C	19.929887	18.794719
a_0	42877.775	48561.865
a_1	−20381.321	−29552.482
a_2	9660.8179	13479.764
a_3	−1862.7119	−2369.8453

However, the long-term creep data do show a substantial improvement in creep performance of the weldment in comparison to aging alone. There are likely multiple reasons for this improvement. First, the solution annealing results in a uniform γ′distribution in the weldment and between the weldment and the base metal as shown in the hardness data and testing at lower temperatures. This decreases the strain inhomogeneity during creep which may occur from modest variations in γ′size and distribution between weld passes and the weld metal and base metal. Second, the solution annealing cycle may not have been sufficient to eliminate all microstructural gradients in the weld. Solidification and diffusion modeling of alloy 740H weld metal confirms that Ti and Nb are the strongest elements for segregation in alloy 740H and for a dendrite arm spacing of 7.5 μm, it has been suggested that full homogenization of an alloy 740H single pass weldment requires 4 h at 1100 °C [14]. Large compositional gradients were not observed in this study, but the EDS analysis showing a measurable difference in Nb content between two grains in Fig. 15 (1.7–1.3%) provides some evidence for a small compositional gradient which still exists after solution annealing, aging, and long-term creep. The large creep damage zone in the higher temperature and lower stress tests, which extended throughout the WM to the FL regions, also suggests that the solution annealing eliminated the largest microstructural gradients allowing for subtle difference in microstructural evolution, including γ′coarsening, to accelerate creep in the weldment in comparison to the wrought BM. Since creep damage

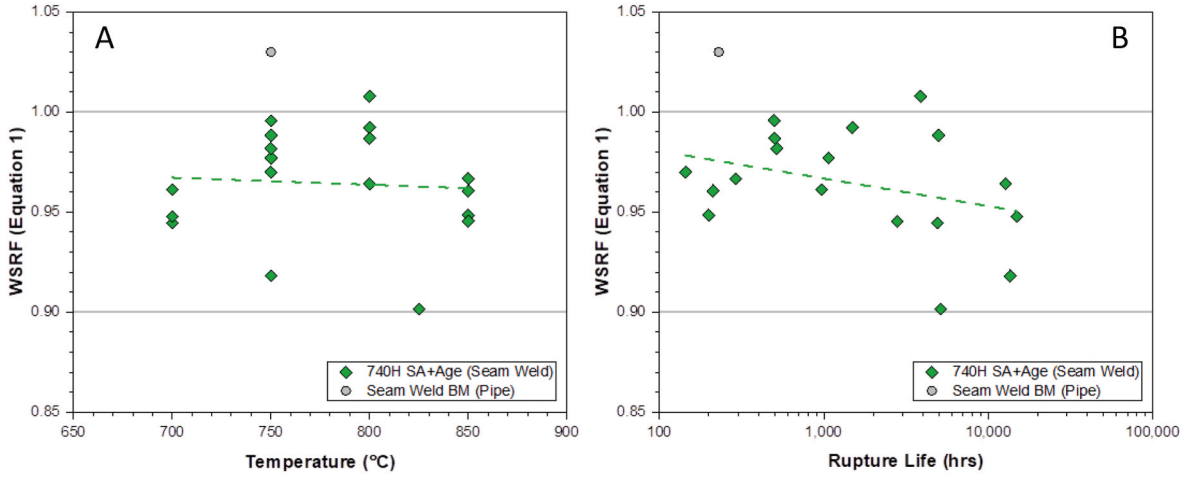

Fig. 14. Individually calculated *WSRF*s for the alloy 740H seam-welded pipe as a function of rupture life (a) and temperature (b).

Table 6
Extrapolated stress to produce 100,000 h average rupture life (equation (2) and Table 5).

Temperature (°C)	Base Metal (MPa)	Weldment (MPa)	*WSRF* (equation (1))
700	215	192	0.9
725	164	144	0.9
750	121	104	0.9
775	85.4	74.1	0.9
800	58.4	52.9[a]	0.9
825	39.6	38.8[a]	1.0

[a] Denotes stresses which are below minimum applied stress in the database.

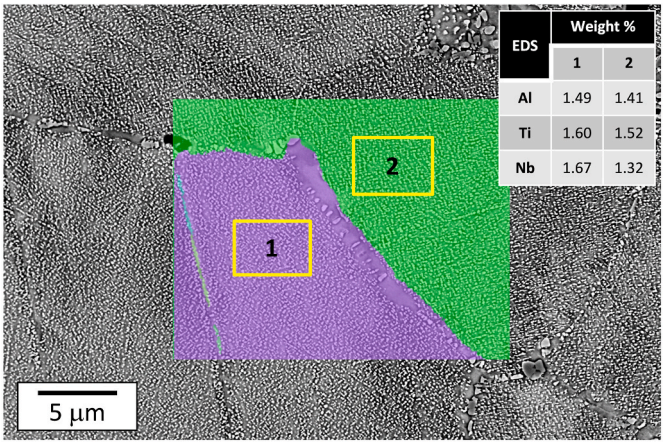

Fig. 15. EBSD orientation map overlayed on BSE image of an alloy 740H grain boundary after creep testing with inlayed EDS area spectrum for two grain interiors.

was not observed in the BM, all WM creep-rupture tests could be conducted in the future to further explore the specific creep deformation mechanisms in the WM to compare to available mechanistic data on the BM [39] which suggests a grain boundary sliding mechanism occurring within the power-law creep regime. Additionally, such research could lead to strategies for futher WM high-temperature performance improvements such as higher-temperature solution annealing temperatures and/or longer times as previously suggested by Bechetti [14–16] or alternative WM chemistries.

6. Conclusions

A full-scale industrial trial produced a high-quality minimal defect first-of-a-kind alloy 740H seam welded pipe. Unlike previous work on alloy 740H weldments, this seam weld was subject to a solution annealing + aging heat-treatment after welding. Extensive time independent testing showed the component met all the specification requirements and supplementary testing confirmed good tensile strength, ductility, and impact properties. High-temperature low-cycle fatigue and creep testing were conducted. The fatigue performance was at the bottom of the wrought alloy scatterband with failure initiation in the WM. Multiple analysis methods applied to the creep data concluded a *WSRF* of 0.9 was appropriate and conservative for pressure part design. This small performance debit is a significant improvement over the current *WSRF* for alloy 740H of 0.7 for welded + aged weldments. Detailed metallurgical investigations showed long-term creep damage occurred in the WM due to discontinuous γ′coarsening reactions leading to CZ where creep cavities initiated in γ′ denuded regions. The research suggests the solution annealing conditions selected for this research did not completely homogenize the microstructure with subtle compositional gradients and microstructural features leading to the formation of the CZs.

Author statement

John Shingledecker: Conceptualization, Methodology, Formal analysis, Investigation, Visualization, Writing – original draft, Writing – review & editing, Supervision. John deBarbadillo: Conceptualization, Methodology, Investigation, Writing – review & editing. Ronald Gollihue: investigation, Resources. Eeva Griscom: investigation, Visualization, Writing – original draft. Daniel Purdy: Investigation, Formal analysis, Writing – review & editing. Alex Bridges: Formal analysis.

Disclaimer

This report was prepared as an account of work sponsored by an agency of the United States Government. Neither the United States Government nor any agency thereof, nor any of their employees, makes any warranty, express or implied, or assumes any legal liability or responsibility for the accuracy, completeness, or usefulness of any information, apparatus, product, or process disclosed, or represents that its use would not infringe privately owned rights. Reference herein to any specific commercial product, process, or service by trade name, trademark, manufacturer, or otherwise does not necessarily constitute or imply its endorsement, recommendation, or favoring by the United States Government or any agency thereof. The views and opinions of authors expressed herein do not necessarily state or reflect those of the United States Government or any agency thereof."

Declaration of competing interest

The authors declare that they have no known competing financial interests or personal relationships that could have appeared to influence the work reported in this paper.

Data availability

All data are tabulated in the manuscript and/or are available from the provided references

Acknowledgements

This material is based upon work supported by the U.S. Department of Energy Office of Energy Efficiency and Renewable Energy (EERE) under the Solar Energy Technologies Office Award Number DE-EE0008367 and the guidance of Kamala Raghaven is appreciated. The collaboration with Anthony Long, Swepco Tube, Llc, is acknowledged. The support of the experimental work from Kendall McCord and Adam Combs, EPRI, and the advice and guidance of John Siefert and Tapasvi Lolla, EPRI, is also acknowledged.

References

[1] John P. Shingledecker, John A. Siefert. "Age Hardenable Nickel-based Alloy Developments and Research for New High Temperature Power Cycles." In Ott E. et al. (eds) *Proceedings of the 9th International Symposium on Superalloy 718 & Derivatives: Energy, Aerospace, and Industrial Applications*, © 2018 The Minerals, Metals & Materials Series. Springer, Cham. https://doi.org/10.1007/978-3-319-89480-5_1.
[2] INCONEL Alloy 740H" *Chapter 14*: Materials for Ultra-supercritical and Advanced Ultra-supercritical Power Plants © 2017, Elsevier Ltd., UK. ISBN: 978-08-100552-1.
[3] R. Viswanathan, J.F. Henry, J. Tanzosh, G. Stanko, J. Shingledecker, B. Vitalis, R. Purgert, J. Mater. Eng. Perform. 14 (2005) 281.
[4] John Shingledecker, John deBarbadillo, Dave O'Donnel, Steve McCoy, Brian Baker, Stephen Coryell, Materials improvements for improved economy of high-temperature components in future gen 3 CSP systems." *Proceedings to SolarPACES2018*. October 2-5, 2018. Casablanca, Morocco, AIP Conf. Proc. 2126 (2019), 020004.
[5] Case 2702-6." *BPVC Code Cases: Boilers And Pressure Vessels*, BPVC-CC-BPV-2021, 2021, ISBN 9780791874325. ASME.
[6] Case 3056." *BPVC Code Cases: Boilers And Pressure Vessels*, BPVC-CC-BPV-2021, ASME, 2022.
[7] Case 190-3, *Power Piping*. B31.1-2022, ASME, 2022, ISBN 9780791875292.

[8] Case 7-1." *Valves—Flanged, Threaded, and Welding End*. B16.34-2020, ASME, 2021, ISBN 9780791873809.
[9] John deBarbadillo, Brian Baker, Ronald Gollihue, Steve McCoy, John Shingledecker, Dan Purdy, Recent developments in manufacturing and fabrication of alloy 740H components for sCO2 applications, February 21 – 24, The 7th International Supercritical CO2 Power Cycles Symposium (2022). San Antonio, Texas. Paper #165, https://sco2symposium.com/proceedings2022/165-paper.pdf.
[10] Robert Purgert, John Shingledecker, James Pschirer, Reddy Ganta, Paul Weitzel, Jeff Sarver, Peter Tortorelli, Boiler Materials for Ultra Supercritical Coal Power Plants, 2015, https://doi.org/10.2172/1346714. United States.
[11] J.P. Shingledecker, Creep-rupture performance of INCONEL alloy 740H and welds, Oct. 22-25, in: Advances in Materials Technology for Fossil Power Plants. Proceedings from the Seventh International Conference, 2013. Waikoloa, Hawaii USA. Published by ASM International © 2014. EPRI Report Number 3002002375. 230-241.
[12] J.A. Siefert, J.P. Shingledecker, J.N. Dupont, S.A. David. "Weldability and weld performance of candidate nickel base superalloys for advanced ultrasupercritical fossil power plants part II: weldability and cross-weld creep performance." Sci. Technol. Weld. Join. Available online October 2015. http://doi.org/10.1179/1362171815Y.0000000094.
[13] Kinga A. Unocic, Xiang Chen, Peter F. Tortorelli. "Microstructural Evaluation of Welded Nickel-Based Superalloy Inconel 740H After Creep Testing." JOM, Vol. 72, No. 5 ©2020 The Minerals, Metals & Materials Society. https://doi.org/10.1007/s11837-020-04119-2.
[14] D.H. Bechetti, J.N. DuPont, J.J. deBarbadillo, et al., Homogenization and dissolution kinetics of fusion welds in INCONEL® alloy 740H, Metall. Mater. Trans. A 45 (2014) 3051–3063, https://doi.org/10.1007/s11661-014-2243-z.
[15] D.H. Bechetti, J.N. DuPont, J.J. de Barbadillo, et al., Microstructural evolution of INCONEL® alloy 740H® fusion welds during creep, Metall. Mater. Trans. A 46 (2015) 739–755, https://doi.org/10.1007/s11661-014-2682-6.
[16] D.H. Bechetti, J.N. Dupont, M. Watanabe, et al., Characterization of discontinuous coarsening reaction products in INCONEL® alloy 740H® fusion welds, Metall. Mater. Trans. A 48 (2017) 1727–1743, https://doi.org/10.1007/s11661-016-3952-2.
[17] D.H. Bechetti, J.N. DuPont, J.A. Siefert, et al., Microstructural evolution and creep-rupture behavior of A-USC alloy fusion welds, Metall. Mater. Trans. A 47 (2016) 4502–4518, https://doi.org/10.1007/s11661-016-3603-7.
[18] Sklenička Václav, Květa Kuchařová, Milan Svoboda, Marie Kvapilová, Petr Král, Jiří Dvořák, Creep behaviour of IN 740 alloy after HAZ thermal cycle simulations, Int. J. Pres. Ves. Pip. 178 (2019), 104000, https://doi.org/10.1016/j.ijpvp.2019.104000. ISSN 0308-0161.
[19] ASTM B775/B775M-19, Standard Specification for General Requirements for Nickel and Nickel Alloy Welded Pipe, ASTM International, 2019.
[20] *BPVC Section VIII-Rules For Construction Of Pressure Vessels*. BPVC-VIII-2021, ASME, 2021, ISBN 9780791874233.
[21] ASTM E213-02/ISG-UT 500 Rev. 10, Standard Practice for Ultrasonic Testing of Metal Pipe and Tubing, ASTM International, 2002.
[22] Brazing Bpvc Section IX-Welding, Fusing Qualifications, BPVC-IX-2021, ASME, 2021, ISBN 9780791874264.
[23] Standard Test Methods for Tension Testing of Metallic Materials, ASTM E8/E8M, ASTM International, 2022.
[24] ASTM E606/E606M-21, Standard Test Method for Strain-Controlled Fatigue Testing, ASTM International, 2021.
[25] ASTM E139-11(2018, Standard Test Method for Conducting Creep, Creep-Rupture, and Stress-Rupture Tests of Metallic Materials, ASTM International, 2018.
[26] Storesund Jan, Shan Tung Tu, Geometrical effect on creep in cross weld specimens, Int. J. Pres. Ves. Pip. 62 (Issue 2) (1995) 179–193, https://doi.org/10.1016/0308-0161(94)00009-8. ISSN 0308-0161.
[27] Fujimitsu Masuyama, Effect of specimen size and shape on creep rupture behavior of creep strength enhanced ferritic steel welds, Int. J. Pres. Ves. Pip. 87 (Issue 11) (2010) 617–623, https://doi.org/10.1016/j.ijpvp.2010.08.006. ISSN 0308-0161.
[28] J.A. Siefert, J.D. Parker, R. Thomson, Cross-weld creep performance in grade 91 steel: macro-based assessment, Weld. J. (2019), https://doi.org/10.29391/2019.98.005. American Welding Society, March.
[29] L.H. Sjodahl, A comprehensive method of rupture data analysis with simplified models, Characterization of Materials for Service at Elevated Temperatures (1978) 501–514. MPC-7, ASME, New York, NY.
[30] Creep Rupture Assessment Handbook: A Procedure Guide, EPRI, Palo Alto, CA, 2020, 3002016956.
[31] J. Shingledecker, N. Evans, G. Pharr, Mater. Sci. Eng. A 578 (2013) 277–286.
[32] M. Render, M.L. Santella, X. Chen, et al., Long-term creep-rupture behavior of alloy Inconel 740/740H, Metall. Mater. Trans. A 52 (2021) 2601–2612, https://doi.org/10.1007/s11661-021-06253-1.
[33] Design Guidance for High Temperature Concentrating Solar Power Components, ANL-20/03.,.
[34] S. Zhang, Y. Takahashi, Creep and Creep-Fatigue Deformation and Life Assessment of Ni-Based Alloy 740H and Alloy 617, July 15-20, 2018, pp. PVP2018–85079 (Prague, Czech Republic).
[35] Unpublished data obtained via personal communication, Brian Baker, Special Metals Corporation (2021). March.
[36] C. Kumar, P.S.M. Jena, R.K. Singh, G.A. Harmain, J.K. Sahu, Strain ratio effect on microstructural evolution during low cycle fatigue exploitation of nickel base superalloy IN 740H, Int. J. Pres. Ves. Pip. 194 (2021), 104551, https://doi.org/10.1016/j.ijpvp.2021.104551. Part B ISSN 0308-0161.
[37] John Shingledecker, Improving Economics of Generation 3 CSP System Components through Fabrication and Application of High Temperature Nickel-Based Alloys. U.S. DOE, EE-EE0008367, In Publication.
[38] S.A. David, J.A. Siefert, J.N. Dupont, J.P. Shingledecker, Weldability and weld performance of candidate nickel base superalloys for advanced ultrasupercritical fossil power plants part I: fundamentals, Sci. Technol. Weld. Join. 20 (Issue 7) (October 2015) 532–552.
[39] K.A. Unocic, J.P. Shingledecker, P.F. Tortorelli, Microstructural changes in Inconel® 740 after long-term aging in the presence and absence of stress, JOM 66 (2014) 2535–2542, https://doi.org/10.1007/s11837-014-1208-4.